Mechanistic Aspects of Dinitrogen Hydrogenation Catalyzed by the Geometry-Constrained Zirconium and Titanium Complexes: Computational Studies

Sonia Martinez,[†,‡] Keiji Morokuma,[†] and Djamaladdin G. Musaev*[,†]

Cherry L. Emerson Center for Scientific Computation, and Department of Chemistry, Emory University, Atlanta, Georgia 30322, and Departamento de Física Macromolecular, Instituto de Estructura de la Materia, Consejo Superior de Investigaciones Científicas, Serrano 113 Bis, 28006 Madrid, Spain

Received June 20, 2007

We applied the density functional theory to propose a new class of compounds affording hydrogenation of the coordinated dinitrogen molecule under mild conditions. These calculations have demonstrated that geometry-constrained complexes with a formula of $(C_5H_4SiH_2NR)M$, where M = Ti (with R = H(**1**) and Me(**2**)) and Zr (with R= H(**3**), Me(**4**), and ^{t}Bu(**5**)) coordinate the N_2 molecule in a side-on manner and form highly stable (relative to the dissociation limit of 2**n** + N_2) **n**-(μ_2,η^2,η^2-N_2)-**n** dimer (where **n** = **1**−**5**), and satisfy the first necessary condition of hydrogenation of the coordinated N_2 molecule. These complexes also satisfy the second necessary condition for the successful hydrogenation of the side-on coordinated N_2 molecule: they possess appropriate frontier orbitals to add an H_2 molecule. Calculations show that **n**-(μ_2,η^2,η^2-N_2)-**n** complexes add an H_2 molecule with a reasonable barrier (ca. 20, 14−16, and 15−18 kcal/mol for **n** = **1**, **3**, and **4**, respectively); Zr complex **3,** is expected to be more reactive than its Ti analogue **1**. Replacement of R = H in **3** with R= Me (i.e., going from **n** = **3** to **n** = **4**) has no significant effect on the calculated H−H addition barriers. The comparison of the calculated H−H addition barriers of these species with those (18−20 and 24 kcal/mol barriers) for experimentally and computationally well-studied dizirconium complexes $\{[P_2N_2]Zr\}_2(\mu_2,\eta^2,\eta^2\text{-}N_2)$ (where $[P_2N_2]$ = $PhP(CH_2SiMe_2NSiMe_2CH_2)_2PPh$) and $\{(C_5Me_4H)_2Zr\}_2(\mu_2,\eta^2,\eta^2\text{-}N_2)$ show that the proposed complexes **1**, **3**, and **4** will exhibit similar or better reactivity toward the H_2 molecule than the latter complexes.

1. Introduction

Designing novel catalysts that can facilitate the utilization of a N≡N triple bond of an inert and abandoned N_2 molecule under mild conditions have occupied the minds of many scientists for years.[1] Extensive studies[1,2−7] during the past several decades have led to discovery of several important reactions for activation and transformation of N≡N triple bonds and have provided deeper understandings of the fundamental principles of nitrogen fixation via both *protonation-and-reduction* and *hydrogenation* mechanisms. In general, it was demonstrated that the first condition of utilization of the N_2 molecule is its coordination to the transition-metal centers. Since discovery of the $[Ru(NH_3)_5(N_2)]^{2+}$ complex in 1965, a large number of dinitrogen/transition-metal complexes have been synthesized. Detailed structural analysis of this large class of mononuclear transition-metal/N_2 complexes has revealed that the N_2 molecule in this species is mostly in its end-on (η^1) coordination mode (Scheme 1), which is suitable for utilization of the N≡N triple bond via *protonation-and-reduction* (Chatt-type) mechanism.

The side-on (η^2) coordination of N_2 molecule to a transition-metal center with strong M−N_2 interaction, the first necessary condition for its successful *hydrogenation*, is extremely difficult to achieve in mononuclear transition-metal complexes. However, it can be achieved in multinuclear transition-metal complexes. In the literature, numerous dinuclear-dinitrogen complexes, $[L_nM]_2(\mu_2,\eta^2,\eta^2\text{-}N_2)$, with a side-on ($\eta^2$) coordinated N_2, were reported. However, extensive studies[1,3,6,8,9] of the reactivity of these complexes have shown that not every reported $[L_nM]_2$-(μ_2,η^2,η^2-N_2) complex with a side-on coordinated N_2 molecule adds hydrogen molecule to N_2. On the basis of these studies it is concluded that, in addition to the side-on coordination of N_2, there are other factors that control the successful hydrogenation of N_2 molecule.

One of these critical factors is the availability of the singlet electronic state of these complexes with appropriate frontier orbitals: HOMO, which is expected to donate electrons to the σ_u* orbital of the reacting H_2 molecule and should be a π-bonding orbital of M−N_2−M fragment.[2,10] Meanwhile, the

[†] Emory University.

[‡] Instituto de Estructura de la Materia, Consejo Superior de Investigaciones Científicas.

(1) (a) Fryzuk, M. D.; Johnson, S. A. *Coord. Chem. Rev.* **2000**, *200*−*202*, 379. (b) Jennings, J. R., Ed. *Catalytic Ammonia Synthesis*; Plenum: New York, 1991. (c) Fryzuk, M. D. *Nature* **2004**, *427*, 498. (d) Schlögl, R. *Angew. Chem., Int. Ed.* **2003**, *42*, 2004. (e) Mori, M. *J. Organomet. Chem.* **2004**, *689*, 4210. (g)Yandulov, D. V.; Schrock, R. R. *Science* **2003**, *76*, 301. (h) Schrock, R. R. *Acc. Chem. Res.* **2005**, *38*, 955. (i) MacKay, B. A.; Fryzuk, M. D. *Chem. Rev.* **2004**, *104*, 385. (j) Gambarotta, S.; Scott, J. *Angew. Chem., Int. Ed.* **2004**, *43*, 5298.

(2) Bobadova-Parvanova, P.; Wang, Q.; Quinonero-Santiago, D.; Morokuma, K.; Musaev, D. G. *J. Am. Chem. Soc.* **2006**, *128*, 11391.

(3) Musaev, D. G. *J. Phys. Chem. B* **2004**, *108*, 10012.

(4) Basch, H; Musaev, D. G.; Morokuma, K. *Organometallics* **2000**, *19*, 3393.

(5) Musaev, D. G.; Basch, H.; Morokuma, K. *Computational Modeling of Homogeneous Catalysis*; Kluwer Academic Publishers: Norwell, MA, 2002.

(6) MacLachlan, E. A.; Fryzuk, M. D. *Organometallics* **2006**, *25*, 1530, and references therein.

(7) Bernskoetter, W. H.; Lobkovsky, E.; Chirik, P. J. *J. Am. Chem. Soc.* **2005**, *127*, 14051.

(8) Chirik, P. J.; Henling, L. M.; Bercaw, J. E. *Organometallics* **2001**, *20*, 534.

(9) Chirik, P. J. *Dalton Trans.* **2007**, 16−25.

10.1021/om700613v CCC: $37.00
Publication on Web 10/25/2007

Scheme 1. End-on (η^1) and Side-on (η^2) Coordination Modes of N_2 to One and Two Transition Metal Centers

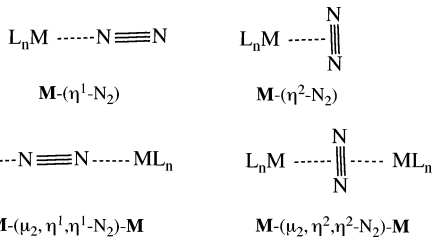

Scheme 2. Schematic Presentation of the Metathesis Transition State, H-bridged Product and Non-H-bridged Product of the Reaction of H_2 Molecule with L_nM-(μ_2,η^2,η^2-N_2)-ML_n Complex

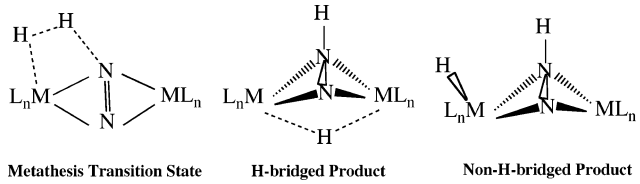

LUMO of these complexes, which accepts electrons from the σ_g-bonding MO of the reacting H_2 molecule, should mainly have a metal character. This qualitative orbital picture is consistent with the "metathesis" transition state (that involves one of the M and N atoms of the complex, and two H atoms of the H_2 molecule, see Scheme 2) reported for H_2 addition to di-zirconium-N_2, $[L_nZr]_2(\mu_2,\eta^2,\eta^2\text{-}N_2)$, complexes.[2−4,11−14]

Another critical factor for *successful addition of several (consequent)* H_2 molecules to the side-on coordinated N_2 is geometrical rigidity[2] of L_n ligands of M centers. It was shown that the rigid (nonflexible) ligand environment of M centers prevents the formation of a H-bridged [with a M(μ_2-H)(μ_2,η^2,η^2-NNH)M moiety] intermediate after the first H_2 addition. The addition of the H_2 molecule to the H-bridged intermediate requires a larger energy barrier than that to the intermediate without a H-bridged structure [with a HM(μ_2,η^2,η^2-NNH)M moiety] (see Scheme 2).

Recent studies have shown that dinuclear complexes $[L_nM]_2$-(μ_2,η^2,η^2-N_2) of group IV transition metals (Zr and Hf) with {PhP($CH_2SiMe_2NSiMe_2CH_2$)PPh}[15] and (η^5-C_5Me_4H)[16] ligands add dihydrogen molecule to the coordinated N_2 under mild experimental conditions. In early studies[17] it was shown that multi-hapto ligand η^5:η^1-$C_5H_{5-n}Me_nSiR'_2NR$ offers steric and electronic requirements, which can be compared to and contrasted with those of more conventional Cp_2 ligands. In fact, the resulting ($C_5H_{5-n}Me_nSiR'_2NR$)M complexes of group IV transition metals (called "constrained-geometry catalysts"), which are widely used in homogeneous catalysis (for example, for olefin polymerization), show reactivity similar to that of their metallocene analogues.[18,19] Therefore, in the present contribution we propose to study structure, stability, and reactivity (toward H_2 molecule) of (Cp′SiH_2NR)M-(μ_2,η^2,η^2-N_2)-M(Cp′SiH_2NR) complexes aiming to find a more efficient dinitrogen-hydrogenation reaction. In our studies we use M = Ti and Zr, R = H, Me, and ^{t}Bu, and Cp′ = Cp and Ind, (see Scheme 3). In the first part of the present paper, we elucidate geometry and controlling factors of relative stability of side-on vs end-on N_2 coordination modes in the proposed mononuclear, (Cp′SiH_2-NR)M(N_2), and dinuclear, [(Cp′SiH_2NR)M]$_2$(N_2), complexes. In the second part, we investigate the mechanism of the reaction of selected $[Cp'SiH_2NR)M]_2(\mu_2,\eta^2,\eta^2\text{-}N_2)$ complexes with the H_2 molecule.

Scheme 3. Schematic Presentation of Complexes Used in the Present Study; the Calculated, Important Geometry Parameters and Relative Energies (of Lower-Lying Electronic States) of These Complexes Are Presented in Table 1

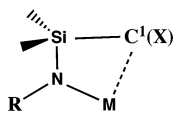

1 M = Ti; R = H; X = Cp
2 M = Ti; R = Me; X = Cp
3 M = Zr; R = H; X = Cp
4 M = Zr; R = Me; X = Cp
5 M = Zr; R = ^{t}Bu; X = Cp
6 M = Zr; R = H; X = Ind

2. Computational Procedure

The geometries of all the proposed complexes, as well as reactants, intermediates, transition states, and products of the proposed reactions with the H_2 molecule, were optimized using the hybrid density functional B3LYP method[20] and Stevens−Basch−Krauss (SBK)[21] relativistic effective core potentials (for Ti, Zr, Si C, and N). We used standard CEP-31G basis sets for all atoms, augmented with d-type polarization functions (α = 0.80 (N) and 0.55 (Si)) for N and Si atoms, respectively. Below we denote this method as B3LYP/CEP-31G($d_{N,Si}$). Since this is the same method that was used previously in our studies, one can directly compare the presented new findings with those from our previous studies. All reported structures were optimized without any symmetry constraints, and their nature was confirmed by performing normal-mode analysis. In addition, we performed intrinsic reaction coordinate (IRC) calculations for all located transition states to confirm the reactants and products connected by these transition states. All reported results were calculated by using the Gaussian_03 program package.[22]

Recently, for $[(\eta^5\text{-}C_5Me_nH_{5-n})_2M]_2(\mu_2,\eta^2,\eta^2\text{-}N_2)$ (where n = 0 and 4) complexes of group IV transition metals, we have demonstrated[10] the importance of the low-lying electronic states of reactants for the reaction of coordinated N_2 with H_2. It was shown

(10) Musaev, D. G.; Bobadova-Parvanova, P.; Morokuma, K. *Inorg. Chem.* **2007**, *46*, 2709.
(11) Basch, H.; Musaev, D. G.; Morokuma, K.; Fryzuk, M. D.; Love, J. B.; Seidel, W. W.; Albinati, A.; Koetzle, F.; Klooster, W. T.; Mason, S. A.; Eckert, J. *J. Am. Chem. Soc.* **1999**, *121*, 523.
(12) Basch, H; Musaev, D. G.; Morokuma, K. *J. Am. Chem. Soc.* **1999**, *121*, 5754.
(13) Miyachi, H.; Shigeta, Y.; Hirao, K. *J. Phys. Chem. A* **2005**, *109*, 8800.
(14) Yates, B. F.; Basch, H.; Musaev, D. G.; Morokuma, K. *J. Chem. Theory Comput.* **2006**, *2*, 1298.
(15) Fryzuk, M. D.; Love, J. B.; Rettig, S. J.; Young, V. G. *Science* **1997**, *275*, 1445.
(16) Pool, J. A.; Lobkovsky, E.; Chirik, P. J. *Nature* **2004**, *427*, 527.
(17) (a) Shapiro, P. J.;Bunel, E.; Schaefer, W. P.; Bercaw, J. E. *Organometallics* **1990**, *9*, 867. (b) Shapiro, P. J.; Cotter, W. D.; Schaefer, W. P.; Labinger, J. A.; Bercaw, J. E. *J. Am. Chem. Soc.* **1994**, *116*, 4623 and references therein. (c) Coughlin, E. B.; Shapiro, P. J.; Bercaw, J. E. *Polym. Prepr.* **1992**, *33*, 1226.
(18) Devore, D. D.; Timmers, F. J.; Hasha, D. L.; Rosen, R. K.; Marks, T. J.; Deck, P. A.; Stern, C. L. *Organometallics* **1994**, *14*, 3132 and references therein.
(19) (a) Woo, T. K.; Margl, P. M.; Lohrenz, J. C. W.; Blochl, P. E.; Ziegler, T. *J. Am. Chem. Soc.* **1996**, *118*, 13021 and references therein. (b) Lanza, G.; Fragala, I. L.; Marks, T. J. *Organometallics* **2002**, *21*, 5594 and references therein.
(20) (a) Becke, A. D. *Phys. Rev. A* **1988**, *38*, 3098. (b) Lee, C.; Yang, W.; Parr, R. G. *Phys. Rev. B* **1988**, *37*, 785. (c) Becke, A. D. *J. Chem. Phys.* **1993**, *98*, 5648.
(21) (a) Stevens, W. J.; Basch, H.; Krauss, M. *J. Chem. Phys.* **1984**, *81*, 6026. (b) Stevens, W. J.; Krauss, M.; Basch, H.; Jasien, P. G. *Can. J. Chem.* **1992**, *70*, 612. (c) Cundari, T. R.; Stevens, W. J. *J. Chem. Phys.* **1993**, *98*, 5555.
(22) Frisch, M. J.; et al. *Gaussian 03*, revision C.02; *Gaussian, Inc.*: Wallingford CT, 2004.

Table 1. Calculated, Important Geometry Parameters (distances in Å, and angles in deg) at Their Lowest Singlet and Triplet States, as Well as the Energy Difference between the Lowest Singlet (*S*) and Triplet (*T*) States, $\Delta E(S - T)$, (in kcal/mol) of Compounds 1−6

					geometry parameters							
complex	M	R	X	state	M−N	N−R	N−Si	Si−C^1	M−C^1	∠MNSi	∠NSiC^1	$\Delta E(S-T)$
1,	Ti	H	Cp	S	1.941	1.024	1.809	1.909	2.054	94.0	93.3	15.9
				T	1.970	1.025	1.798	1.916	2.256	99.3	94.2	0.0
2,	Ti	Me	Cp	S	1.935	1.482	1.815	1.903	2.055	93.1	94.1	15.5
				T	1.965	1.484	1.802	1.911	2.254	98.3	95.0	0.0
3,	Zr	H	Cp	S	2.051	1.026	1.810	1.904	2.487	107.6	91.8	9.5
				T	2.087	1.020	1.810	1.913	2.481	105.2	93.6	0.0
4,	Zr	Me	Cp	S	2.045	1.485	1.790	1.901	2.493	108.3	91.9	4.5
				T	2.064	1.490	1.811	1.905	2.506	106.1	93.6	0.0
5,	Zr	^{t}Bu	Cp	S	2.049	1.485	1.777	1.906	2.591	110.3	90.4	2.9
				T	2.097	1.488	1.777	1.915	2.481	106.7	93.0	0.0
6,	Zr	H	Ind	S	2.062	1.026	1.793	1.903	2.424	105.5	92.4	7.6
				T	2.082	1.025	1.797	1.912	2.420	103.1	94.5	0.0

that the triplet state (which was found to be the ground state for Ti-complexes) is less (or non-) reactive than the corresponding singlet state (which was found to be the ground state for Zr- and Hf-complexes). Therefore, in the present paper we also investigate the nature of ground electronic states of the proposed complexes.

In general, it is known that the B3LYP functional (used throughout this paper) overstabilizes the high-spin states of transition-metal complexes.[23] Therefore, the B3LYP-calculated energy difference between the lowest singlet and triplet electronic states of the complexes, $\Delta E(S - T)$, presented in this paper should be used with caution and applied only to qualitatively determine the ground electronic state of the proposed species. One should note that the best method to calculate accurate values of $\Delta E(S - T)$ is a highly correlated methods such as CCSD(T) and MRSD-CI with a very large basis set. However, the application of such sophisticated methods to transition-metal complexes proposed in this paper is not practical.

Previously, we have shown[2] that the use of large basis sets (such as Stuttgart/Dresden effective core potential and associated basis sets (SDD)[24] for transition metals in conjunction with the standard 6-31G(d) basis set for the remaining atoms) has no significant effect on the B3LYP/CEP-31G($d_{N,Si}$)-calculated geometries and energetics of the reactants, transition states, intermediates and products of the reaction of $[(\eta^5\text{-}C_5Me_nH_{5-n})_2M]_2(\mu_2,\eta^2,\eta^2\text{-}N_2)$ with H_2 molecule. Therefore, in the present study we use only B3LYP/CEP-31G($d_{N,Si}$) method.

Throughout the paper the energies (ΔH) obtained at the B3LYP/CEP-31G($d_{N,Si}$) level with zero-point vibrational (ZPV) and thermal corrections (at 298.15 K and 1 atm) are used for the studied reactions. Here, we do not discuss entropy corrections (although we have calculated Gibbs free energies for all reported structures, see Supporting Information) because these corrections are usually significantly (very often unrealistically) large in the gas-phase (model) studies compared to those in solution phase where the real processes are expected to occur. The inclusion of entropy effects in the gas-phase studies could lead to wrong conclusions for solution chemistry. The bulk solvent effects on relative energies of reactants, intermediates, transition states, and products of the proposed reactions were evaluated at the polarizable continuum model (PCM)[25] level using their gas-phase optimized structures and water as a solvent.

(23) Khavrutskii, I. V.; Musaev, D. G.; Morokuma, K. *Inorg. Chem.* **2003**, *42*, 2606 and references therein.

(24) (a) Fuentealba, P.; Preuss, H.; Stoll, H.; Szentpaly, L. V. *Chem. Phys. Lett.* **1989**, *89*, 418. (b) Wedig, U.; Dolg, M.; Stoll, H.; Preuss, H. In *Quantum Chemistry: The Challenge of Transition Metals and Coordination Chemistry*; Veillard, A., Ed.; Reidel: Dordrecht, 1986; p 79. (c) Leininger, T.; Nicklass, A.; Stoll, H.; Dolg, M.; Schwerdtfeger, P. *J. Chem. Phys.* **1996**, *105*, 1052. (d) Cao, X. Y.; Dolg, M. *J. Mol. Struct. (THEOCHEM)* **2002**, *581*, 139.

(25) (a) Tomasi, J.; Persico, M. *Chem. Rev.* **1994**, *94*, 2027−2094. (b) Cammi, R.; Tomasi, J. *J. Comput. Chem.* **1996**, *16*, 1449−58.

3. Results and Discussion

First, let us discuss electronic and geometrical structures of the proposed complexes. For simplicity of our discussion, let us divide these complexes into three classes. Class I includes complexes **1** (R = H) and **2** (R= Me) with formula of ($CpSiH_2$-NR)Ti. Class II includes the ($CpSiH_2NR$)Zr-compounds with R = H (**3**), Me (**4**), and ^{t}Bu (**5**). Comparison of the calculated properties of these complexes within the same class as well as similar systems from different classes will allow us to elucidate the role of the transition-metal center (M) and R ligand in the structure, stability, and reactivity of these geometry-constrained compounds. We also study the complex **6** (Class III) with M = Zr, R = H, and X = indenyl (Ind). Comparison of the results for this compound with those for complex **3** will allow us elucidate the role of X (Cp vs Ind) group in the structure, stability, and reactivity.

3.1. Geometrical and Electronic Structures of the Complexes 1−6. B3LYP calculations of the singlet (S) and triplet (T) states of the complexes **1**−**6** show that their ground electronic states are triplet states with two unpaired electrons located on the M centers. Their singlet states are 2.9−15.9 kcal/mol higher in energy (see Table 1).

The calculated important geometry parameters of these compounds also are presented in Table 1. As seen from this table, S-to-T conversion slightly elongates M−N(amido) bond distance for both Ti- and Zr-complexes. It also causes ca. 0.20 Å elongation of Ti−C^1 (Ti−Cp) distance. For the Zr-complex, the S-to-T excitation does not change Zr−C^1 bond distances for complexes **3**, **4**, and **6**, but it does reduce it by 0.11 Å for complex **5**. It appears that Ind ligand coordinates to the Zr center

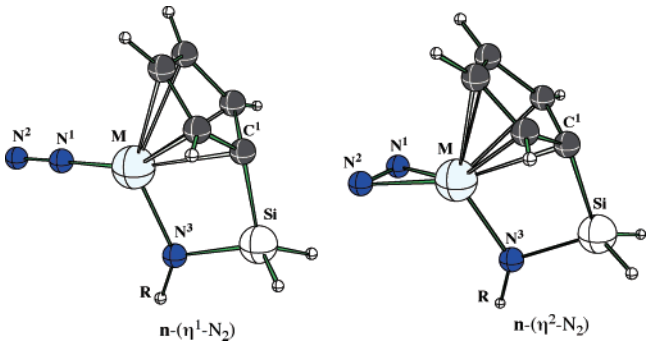

Figure 1. Schematic presentation of the mononuclear **n**-(η^1-N_2) and **n**-(η^2-N_2) complexes (where n = **1**−**6**). The calculated, important geometry parameters and relative energies of these complexes are presented in Table 2.

Table 2. Calculated, Important Geometry Parameters (distances in Å, and angles in deg, see also Figure 1) and Energetics (in kcal/mol) of the n-(η^1-N_2) and n-(η^2-N_2) Complexes, Where $n = 1-6$

		geometry parameters									
complex	state	N^1-N^2	$M-N^1$	$M-N^2$	$M-N^3$	N^3-R	N^3-Si	$Si-C^1$	$M-C^1$	$\Delta E(S-T)^a$	$D_e{}^b$
1-(η^1-N_2),	S	1.179	1.987		1.934	1.024	1.803	1.912	2.176	9.6	11.7
	T	1.185	1.991		1.965	1.025	1.787	1.912	2.329	0.0	5.4
1-(η^2-N_2),	S	1.251	2.049	2.017	1.932	1.024	1.794	1.910	2.334	−2.4	23.2
	T	1.212	2.216	2.180	1.951	1.024	1.786	1.909	2.325	0.0	4.9
2-(η^1-N_2),	S	1.156	2.020		1.926	1.484	1.810	1.906	2.160		12.4
2-(η^2-N_2),	S	1.216	2.031	2.003	1.929	1.485	1.799	1.904	2.328		24.6
3-(η^1-N_2),	S	1.190	2.121		2.082	1.025	1.800	1.913	2.340	7.3	21.6
	T	1.207	2.099		2.089	1.025	1.788	1.911	2.492	0.0	19.4
3-(η^2-N_2),	S	1.234	2.195	2.169	2.073	1.025	1.808	1.907	2.522	−3.9	34.8
	T	1.202	2.333	2.303	2.080	1.025	1.806	1.908	2.489	0.0	21.4
4-(η^1-N_2),	S	1.164	2.159		2.075	1.486	1.805	1.908	2.467		26.0
4-(η^2-N_2),	S	1.229	2.185	2.152	2.073	1.488	1.794	1.904	2.522		39.6
5-(η^1-N_2),	S	1.170	2.158		2.081	1.497	1.800	1.910	2.330		23.9
5-(η^2-N_2),	S	1.225	2.195	2.165	2.086	1.506	1.800	1.905	2.475		36.0
6-(η^1-N_2),	S	1.164	2.147		2.089	1.025	1.791	1.907	2.382		21.3
6-(η^2-N_2),	S	1.226	2.184	2.147	2.084	1.025	1.786	1.906	2.537		34.2

[a] $\Delta E(S-T)$ is an energy difference between singlet and triplet states. [b] D_e is an enthalpy (H) of the reaction **n**-(N_2) → **n** + N_2.

stronger than to the Cp ligand: The calculated $Zr-C^1$ distance, 2.424 Å, is slightly shorter in **6** than that in **3**, 2.487 Å.

3.2. Geometrical and Electronic Structures of the Mononuclear-Dinitrogen Complex, n-(N_2), n = 1−6. In general, the N_2 molecule can coordinate to complexes **1**−**6** in two different ways: in the end-on (η^1) and side-on (η^2) modes (see Figure 1). The calculated important geometry parameters and energetics of the resulting **n**-(N_2) complex are given in Table 2.

As seen from this table, the N−N bond distance is longer in side-on coordinated **n**-(η^2-N_2) isomers than that in their end-on counterparts **n**-(η^1-N_2). This indicates that the N≡N triple bond is more activated in **n**-(η^2-N_2) than in **n**-(η^1-N_2) for all proposed complexes. Furthermore, in the singlet state of **n**-(η^2-N_2) the N−N bond is longer than that in their triplet states (calculated only for $n = 1$ and **3**), indicating that interaction of the N_2 molecule with the M center is slightly stronger in the singlet state compared with that in the triplet state. This conclusion is consistent with the calculated $M-N(N_2)$ bond distances, which are much shorter for singlet complexes than for triplet ones. Changes in the N−N, as well as $M-N(N_2)$ bond distances, upon going from singlet to triplet states of the end-on **n**-(η^1-N_2) complexes are insignificant, indicating weak $M-N_2$ interaction in **n**-(η^1-N_2) complexes.

The above presented geometry changes are consistent with the calculated energy difference between the lowest singlet and triplet states, $\Delta E(S-T)$, and the $M-N_2$ binding energy (D_e). Indeed, as expected, coordination of N_2 to the "naked" complexes **1** and **3** (and presumably for all other studied complexes) stabilizes the singlet state more than their triplet states. As a result, $\Delta E(S-T)$ reduced from 15.9 and 9.5 kcal/mol in the "naked" complexes **1** and **3**, respectively, to 9.6 and 7.3 kcal/mol in the corresponding end-on coordinated complexes **1**-(η^1-N_2) and **3**-(η^1-N_2). Interestingly, in their side-on coordinated analogues **1**-(η^2-N_2) and **3**-(η^2-N_2), strong $M-N_2$ interaction makes the singlet the ground state, and their triplet states lie about 2.4 and 3.9 kcal/mol higher in energy, respectively. Thus, the thermodynamically more stable **n**-(η^2-N_2) isomers of all **n**-N_2 (where $n = 1-6$) complexes studied here have a singlet ground state.

As seen from Table 2, the calculated $M-N_2$ binding energies (D_e) are significantly larger for **n**-(η^2-N_2) isomers than for the **n**-(η^1-N_2) isomers and increase upon going from Ti-complexes to Zr-complexes. It also slightly increases by changing R = H with R = Me and ^{t}Bu. These results indicate that the electron-rich substituent (R) on the amido group of ($CpSiH_2NR$)M-(η^2-N_2) complexes facilitates the activation of the N−N bond of the side-on coordinated N_2 molecule.

Also, one should note that the replacement of Cp ligand by Ind, namely, going from **n** = **3** to **n** = **6**, does not change the calculated $M-N_2$ binding energy.

3.3. Geometrical and Electronic Structures of Dinuclear-Dinitrogen Complex, n-(N_2)-n, n = 1−6. Coordination of the second **n**-complex to mononuclear-dinitrogen complexes **n**-(η^1-N_2) and **n**-(η^2-N_2) leads to dinuclear-dinitrogen complexes **n**-(μ_2,η^1,η^1-N_2)-**n** and **n**-(μ_2,η^2,η^2-N_2)-**n**, respectively. One should note that the side-on coordinated **n**-(μ_2,η^2,η^2-N_2)-**n** complex could have several different isomers, among which *anti*- and *syn*-isomers presented in Figure 2 (and studied only for **n** = **1**, **3**, and **4**) look more interesting from a reactivity point of view (see next section). In the *anti*-isomer two R ligands (or two Cp ligands) are located at *anti* positions to each other. In contrast, in the *syn*-isomer these two ligands are *syn* to each other. Calculations show that these two isomers are energetically very close to each other (with the *anti*-isomer slightly less stable by 0.2, 1.7, and 2.7 kcal/mol for $n = 1$, **3**, and **4**, respectively) and are separated by relatively large energy barriers of 17.0, 12.5, and 13.6 kcal/mol for $n = 1$, **3**, and **4**, respectively. The structures of transition states associated with these barriers are presented in Supporting Information and will not be discussed here. Below, we study structure and reactivity of both isomers.

In Table 3 we present the calculated important geometry parameters and energetics of end-on and side-on isomers of *anti*-**n**-N_2-**n**. As seen in this table, similar to the mononuclear complexes discussed above, the side-on coordination of N_2 to two **n** complexes, *anti*-**n**-(μ_2,η^2,η^2-N_2)-**n**, is significantly more favorable than its end-on coordination. Comparison of corresponding results in Tables 2 and 3 shows that coordination of the second **n** to **n**-(N_2) further stabilizes the singlet state of the resulting species. Indeed, as seen in Table 3, the singlet state of *anti*-**3**-N_2-**3** complex becomes the ground state for both end-on, **3**-(μ_2,η^1,η^1-N_2)-**3**, and side-on, **3**-(μ_2,η^2,η^2-N_2)-**3**, isomers. However, for *anti*-**1**-(μ_2,η^1,η^1-N_2)-**1** the triplet state is still lower (by 8.5 kcal/mol) in energy, while for its side-on coordinated counterpart, *anti*-**1**-(μ_2,η^2,η^2-N_2)-**1,** the singlet state is the ground state. Furthermore, in *anti*-**n**-(μ_2,η^2,η^2-N_2)-**n**, which is the starting complex for addition of the H_2 molecule to the N_2, the N−N bond is significantly elongated (especially for the ground singlet state of these complexes); the calculated N−N distances are within 1.56−1.64 Å range, which corresponds to the N−N single bond. Furthermore, almost all complexes, at their ground

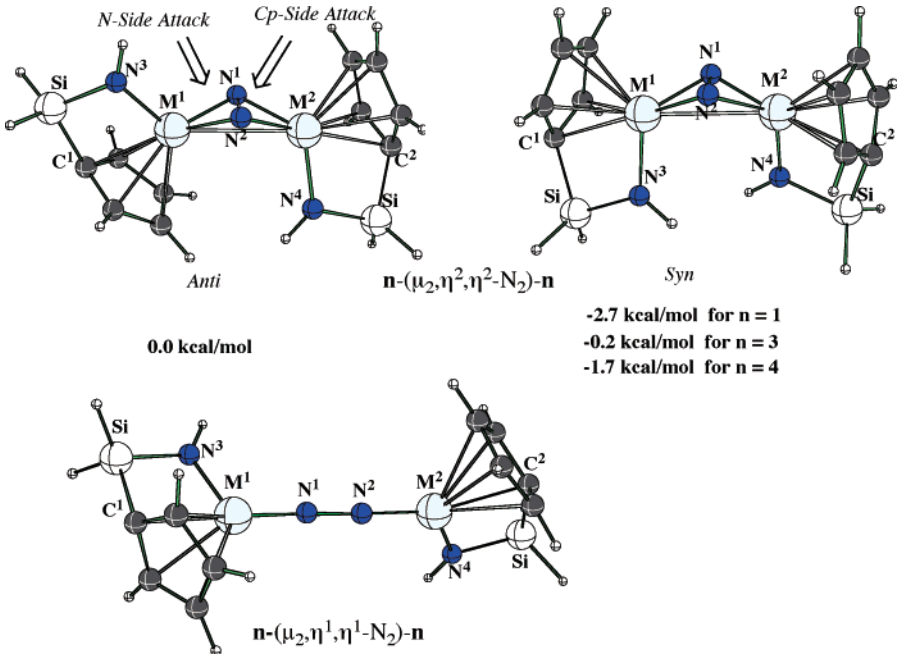

Figure 2. Schematic presentation of the dinuclear **n**-(μ_2,η^2,η^2-N_2)-**n**, *anti*-**n**-(μ_2,η^2,η^2-N_2)-**n**, and *syn*-**n**-(μ_2,η^2,η^2-N_2)-**n** complexes (where $n = \mathbf{1}-\mathbf{6}$). The calculated, important geometry parameters and relative energies of these complexes are presented in Table 3.

Table 3. Calculated, Important Geometry Parameters (distances in Å, and angles in deg, see also Figure 2) and Energetics (in kcal/mol) of the *anti*-n-(μ_2,η^1,η^1-N_2)-n and *anti*-n-(μ_2,η^2,η^2-N_2)-n Complexes, Where $n = 1-6$

		geometry parameters												
complex	state	N^1-N^2	M^1-N^1	M^1-N^2	M^2-N^1	M^2-N^2	M^1-N^3	M^2-N^4	M^1-C^1	M^2-C^2	ϕ_1[a]	ϕ_2[b]	$\Delta E(S-T)$[c]	D_e[d]
1-(μ_2,η^1,η^1-N_2)-**1**	S	1.312	1.752			1.752	1.952	1.957	2.398	2.392	91.6	–	8.5	53.0
	T	1.261	1.925			1.821	1.956	1.947	2.360	2.354	−141.6	---	0.0	51.9
1-(μ_2,η^2,η^2-N_2)-**1**	S	1.639	1.901	1.927	1.944	1.892	1.946	1.951	2.422	2.421	−152.6	42.1	−6.2	57.7
	T	1.353	2.046	2.050	2.046	2.044	1.952	1.957	2.358	2.356	179.7	0.1	0.0	53.9
2-(μ_2,η^1,η^1-N_2)-**2**	S	1.288	1.758			1.758	1.949	1.949	2.386	2.386	−91.0	–		55.1
2-(μ_2,η^2,η^2-N_2)-**2**	S	1.584	2.042	2.058	2.059	2.042	2.103	2.588	2.105	2.585	144.6	36.0		58.2
3-(μ_2,η^1,η^1-N_2)-**3**	S	1.301	1.903			1.904	2.107	2.109	2.551	2.551	−94.3	–	−10.7	74.1
	T	1.270	1.971			2.054	2.087	2.093	2.521	2.527	−109.4	–	0.0	56.1
3-(μ_2,η^2,η^2-N_2)-**3**	S	1.590	2.039	2.054	2.039	2.057	2.109	2.108	2.596	2.594	161.0	42.3	−10.1	88.6
	T	1.329	2.169	2.167	2.167	2.169	2.108	2.108	2.513	2.513	180.0	0.0	0.0	80.4
4-(μ_2,η^1,η^1-N_2)-**4**	S	1.301	1.907			1.907	2.100	2.101	2.549	2.544	−88.5	–		78.5
4-(μ_2,η^2,η^2-N_2)-**4**	S	1.590	2.039	2.054	2.039	2.058	2.111	2.107	2.596	2.594	151.2	39.1		92.5
5-(μ_2,η^1,η^1-N_2)-**5**	S	1.300	1.908			1.908	2.116	2.114	2.527	2.527	−94.1	–		73.2
5-(μ_2,η^2,η^2-N_2)-**5**	S	1.558	2.052	2.057	2.052	2.057	2.124	2.124	2.566	2.566	145.1	0.1		85.0
5-(μ_2,η^1,η^1-N_2)-**5**	S	1.302	1.896			1.895	2.105	2.104	2.572	2.573	−92.1	–		74.5
6-(μ_2,η^2,η^2-N_2)-**6**	S	1.593	2.034	2.054	2.056	2.035	2.103	2.103	2.587	2.598	150.1	43.1		88.6

[a] ϕ_1 is a dihedral angle of $\angle(N^3,M^1,M^2,N^4)$. [b] ϕ_2 is a dihedral angle of $\angle(M^1,M^2,N^1,N^2)$. [c] $\Delta E(S-T)$ is an energy difference between singlet and triplet states. [d] D_e is an enthalpy (H) of the reaction **n**-(N_2)-**n** → **n**-(N_2) + **n**

singlet states, have a "butterfly" structure with the $\phi_1(M^1,M^2,N^1,N^2)$ dihedral angle of 36−42° (with the exception of complex **5**-N_2-**5**, which has a planar M−N_2−M moiety). As seen from this table, the calculated $\phi_1(M^1,M^2,N^1,N^2)$ dihedral angle decreases via **n** = **1** > **2**, and **n** = **3** > **4** > **5**, i.e. via increasing the size of R ligand. This conclusion is consistent with those reported for the dinuclear Zr complex {[P_2N_2]Zr}$_2$(μ_2,η^2,η^2-N_2).[14]

The calculated energy of reaction (involving the same states, singlet or triplet, of the reactants and products) *anti*-**n**-(N_2)-**n** → **n**-(N_2) + **n**, D_e, is large, and is larger for Zr-complexes than for their Ti-analogues.

The *syn*-isomers, *syn*-**n**-(μ_2,η^2,η^2-N_2)-**n,** where two NR ligands (or two Cp ligands) are *syn* to each other were studied only for **n** = **1**, **3**, and **4**. For this isomer, we were able to locate only the structure (presented in Figure 2), where the N_2 molecule is located at the Cp-sides. The structure with N_2 at the RN-side is not stable and converges to the structure presented in Figure 2. The calculated geometries and energies of the *syn*-**n**-(μ_2,η^2,η^2-N_2)-**n** compounds will be discussed in section 3.4.

3.4. Reactivity of the Complexes n-(μ_2,η^2,η^2-N_2)-n toward the Dihydrogen Molecule. The results presented above clearly show that all studied species **n** = **1**, **2**, **3**, **4**, **5**, and **6** coordinate N_2 molecule in side-on manner and form highly stable (relative to dissociation limit of 2**n** + N_2) **n**-(μ_2,η^2,η^2-N_2)-**n** complexes, thus *satisfying the first necessary condition of hydrogenation of the coordinated N_2 molecule*.[2,3,10] Since, as shown above, energy differences between the *anti*- and *syn*-isomers of **n**-(μ_2,η^2,η^2-N_2)-**n** are very small and these isomers are separated with large energy barriers, below we study reaction of both *anti*- and *syn*-**n**-(μ_2,η^2,η^2-N_2)-**n** complexes with the H_2 molecule. We expect that the complexes for all **n**'s studied will show similar reactivity; therefore, here we only investigate reaction mechanisms of **n** = **1**, **3**, and **4** with H_2 molecules in detail.

Before starting our calculations on the potential energy surface of the reaction **n**-(μ_2,η^2,η^2-N_2)-**n** + H_2, we examine the

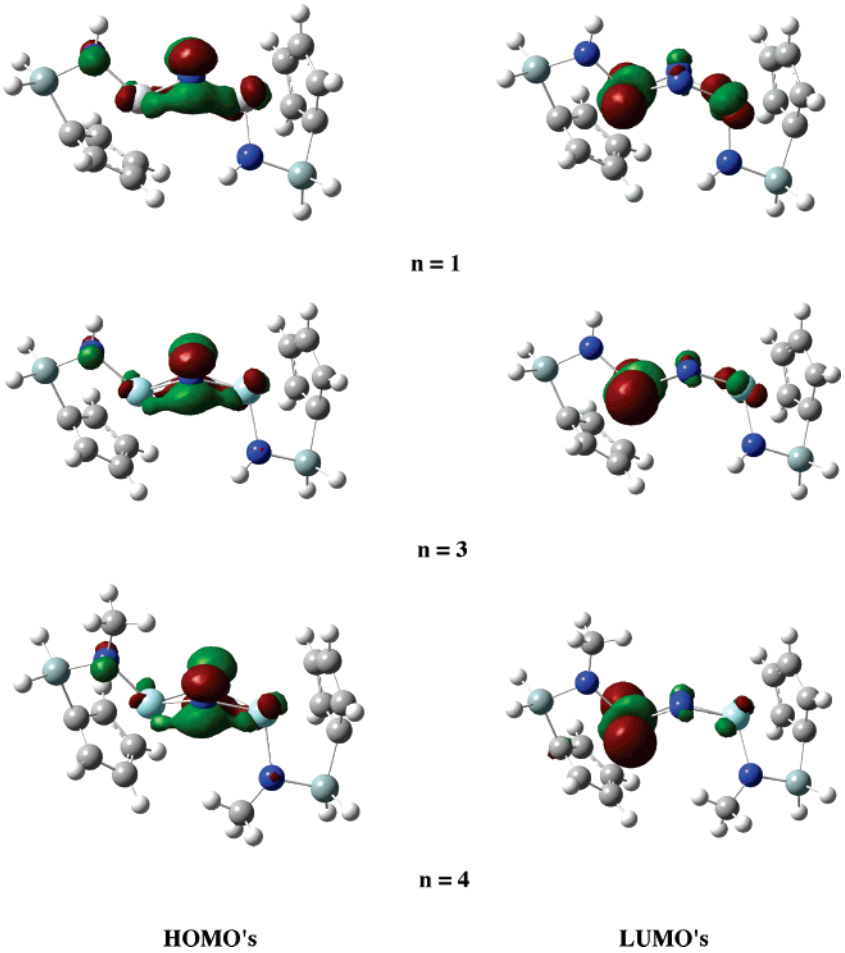

Figure 3. HOMO and LUMO of the *anti*-**n**-(μ_2,η^2,η^2-N_2)-**n** complexes (n = **1**−**3**). Similar orbitals for the *syn*-**n**-(μ_2,η^2,η^2-N_2)-**n** are given in Supporting Information.

applicability of the second necessary condition[2,10] for successful addition of the H_2 molecule. As shown previously (see Introduction), the second necessary condition for the successful hydrogenation of a side-on coordinated N_2 molecule is the availability of the singlet electronic state of the reactant complexes with appropriate frontier orbitals: HOMO should be a π-bonding orbital of the M−N_2−M fragment, while the LUMO should mainly have metal character. As seen in Figure 3, the HOMO and LUMO of the *anti*-**n**-(μ_2,η^2,η^2-N_2)-**n** complex satisfy this requirement. Similar results have been found for the *syn*-**n**-(μ_2,η^2,η^2-N_2)-**n** complex (see Supporting Information). Thus, one may expect that these complexes will add the H_2 molecule to the coordinated N_2 with a reasonable energy barrier.

Now, let us discuss the mechanism and energetics of the reaction **n**-(μ_2,η^2,η^2-N_2)-**n** + H_2. At first, we discuss the mechanism of the reaction of *anti*-**n**-(μ_2,η^2,η^2-N_2)-**n** with the H_2 molecule.

Reactivity of *anti*-n-(μ_2,η^2,η^2-N_2)-n toward the Dihydrogen Molecule. As expected, this reaction proceeds via coordination and activation of the H_2 molecule on one of the M−N bonds through the metathesis transition state (see Scheme 2). As seen in Figure 2, the coming H_2 molecule could coordinate the M−N bond of *anti*-**n**-(μ_2,η^2,η^2-N_2)-**n** from two different directions: from Cp- and N-sides, called below Cp-side and N-side attacks or pathways A and B, respectively. The calculated reactants, transition states, and products of the proposed reactions are presented in Figure 4. Their important geometry parameters and energetics are given in Table 4.

As seen from Table 4, coordination and activation of the H_2 molecule to *anti*-**3**-(μ_2,η^2,η^2-N_2)-**3** occurs with 14.6 and 15.9 kcal/mol barriers at the transition states ***anti*_TS1A_3** and ***anti*_TS1B_3** for pathways A and B, respectively. (Here and below the calculated transition states and products of the reactions are denoted as ***iso*_XYZ_n**, where ***iso*** stands for *anti*- or *syn*-isomers; **X** stands for structure and could be **P** or **TS**, indicating product and transition states, respectively; **Y** corresponds to the number of the hydrogen molecules included in the reaction, and could be **1** or **2**; **Z** stands for the pathways **A** or **B**; and **n** stands for the complex **1**, **3**, or **4**.) The activated H^1−H^2 bond is elongated to 0.953 and 1.067 Å at the transition states ***anti*_TS1A_3** and ***anti*_TS1B_3**, respectively. Meanwhile, the formed N^2−H^1 and Zr^1−/Zr^2−H^2 bond distances are 1.444 and 2.129 Å in ***anti*_TS1A_3**, and 1.353 and 2.014 Å in ***anti*_TS1B_3**, respectively. During this process, the Zr^1−/Zr^2−N^2 bonds are also elongated to 2.183 and 2.185 Å at the transition states ***anti*_TS1A_3** and ***anti*_TS1B_3**, respectively. The optimized geometry parameters indicate that the ***anti*_TS1B_3** is a later transition state than the ***anti*_TS1A_3**, which correlates with the calculated energy of the reaction. IRC calculations indicate that ***anti*_TS1A_3** connects reactants *anti*-**3**-(μ_2,η^2,η^2-N_2)-**3** + H_2 to the product, ***anti*_P1A_3**; reaction **3**-(μ_2,η^2,η^2-N_2)-**3** + H_2 → ***anti*_P1A_3** is calculated to be exothermic by 35.5 kcal/mol. Meanwhile, transition state ***anti*_TS1B_3** connects the reactants *anti*-**3**-(μ_2,η^2,η^2-N_2)-**3** + H_2 to the ***anti*_P1B_3_terminal** product, which lies only 11.4 kcal/mol lower than reactants.

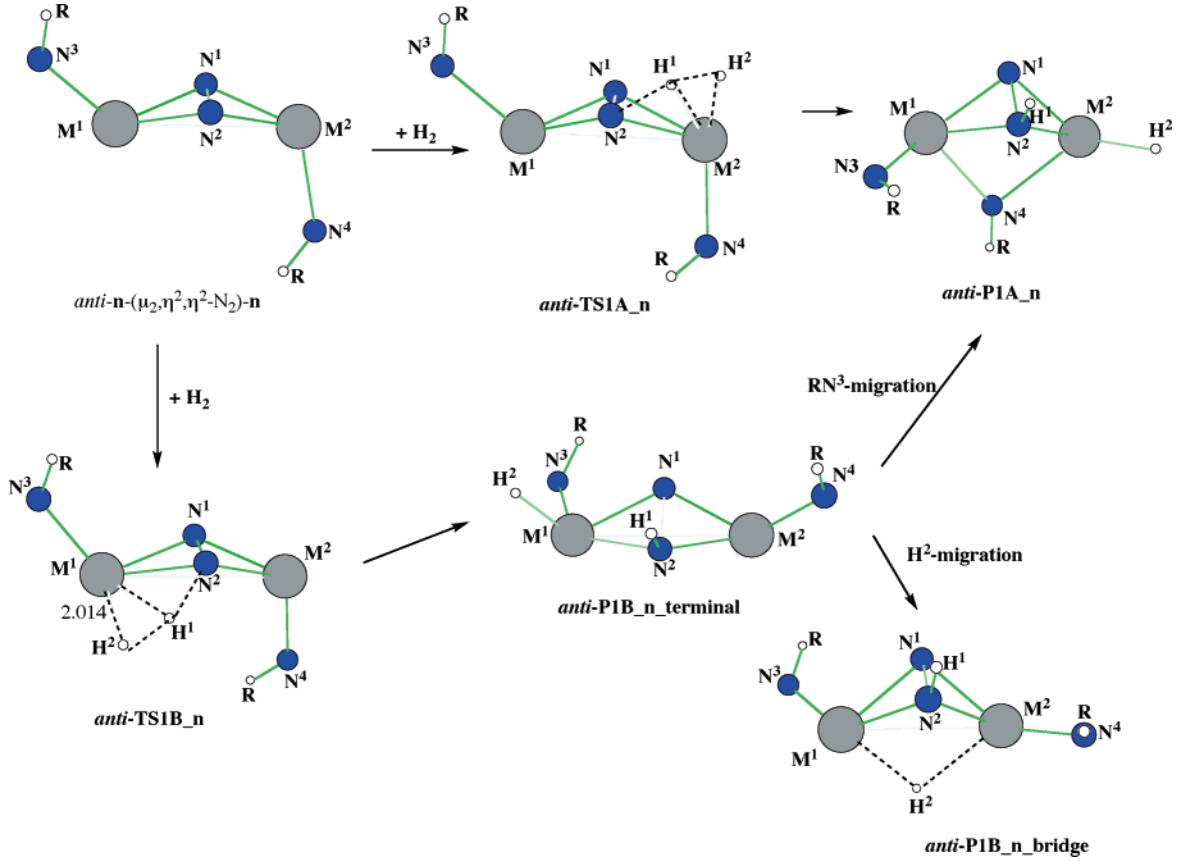

Figure 4. Schematic presentation of the reactants, intermediates, transition states, and products of the reaction of *anti*-**n**-(μ_2,η^2,η^2-N_2)-**n** with H_2 molecule. The calculated, important geometry parameters and relative energies of these complexes are presented in Table 4.

Table 4. Calculated, Important Geometry Parameters (distances in Å, and angles in deg, see also Figure 4), and Relative Energies (in kcal/mol), ΔH (in gas-phase) and ΔG_{Sol} (in water solution), of the Reactants, Transition States, Intermediates, and Products of the Reaction of *anti*-n-(μ_2,η^2,η^2-N_2)-n with H_2 Molecule (where n = 1, 3, and 4)

structure	ΔH	ΔG_{Sol}	M^1-N^1	M^1-N^2	M^1-N^3	M^1-N^4	M^2-N^1	M^2-N^2	M^2-N^4	N^1-N^2	H^1-H^2	N^2-H^1	$M-H^1$	M^1-H^2	M^2-H^2
1-(μ_2,η^1,η^1-N_2)-**1**	0.0	0.0	1.880	1.925	1.955	---	1.939	1.876	1.954	1.509	–	–	–	–	–
TS1A_1	19.8	19.4	1.890	1.893	1.955	---	1.927	2.076	1.952	1.533	0.979	1.370	1.916	–	1.904
P1A_1	−23.0	−30.5	1.967	2.045	1.966	2.135	1.943	2.012	2.172	1.523		1.025	–	–	1.717
TS1B_1	20.0	15.7	1.961	2.120	1.932	---	1.868	1.973	1.951	1.467	1.101	1.299	1.808	1.795	–
P1B_1_terminal	−4.2	−8.4	2.024	2.093	1.957	---	1.852	2.002	1.929	1.573	–	1.033	–	–	1.696
P1B_1_bridge	−15.9	−20.3	2.021	1.981	1.960	---	1.916	2.069	1.967	1.525	–	1.026	–	1.848	1.916
3-(μ_2,η^2,η^2-N_2)-**3**	0.0	0.0	2.039	2.054	2.111	---	2.058	2.039	2.107	1.590	–	–	–	–	–
TS1A_3	14.6	16.8	2.042	2.037	2.110	---	2.058	2.183	2.107	1.617	0.953	1.444	2.104	–	2.130
P1A_3	−35.5	−30.5	2.089	2.185	2.118	2.292	2.056	2.157	2.347	1.513	–	1.023	–	–	1.902
TS1B_3	15.9	18.8	2.104	2.200	2.088	---	2.010	2.105	2.098	1.543	1.067	1.353	1.985	2.014	–
P1B_3_terminal	−11.4	−9.6	2.144	2.295	2.106	---	2.022	2.136	2.087	1.633	–	1.035	–	1.875	–
P1B_3_bridge	−26.9	−18.5	2.143	2.153	2.109	---	2.070	2.209	2.114	1.593	–	1.027	–	2.038	2.109
4-(μ_2,η_2,η_2-N_2)-**4**	0.0	0.0	2.039	2.054	2.111	---	2.058	2.039	2.107	1.590	–	–	–	–	–
TS1A_4	14.8	16.9	2.043	2.041	2.104	---	2.058	2.187	2.111	1.614	0.947	1.453	2.109	–	2.135
P1A_4	−32.4	−31.0	2.118	2.194	2.117	2.307	2.074	2.172	2.351	1.585	–	1.026	–	–	1.902
TS1B_4	15.7	16.1	2.112	2.178	2.081	---	2.012	2.108	2.098	1.551	1.049	1.369	1.997	2.031	–
P1B_4_terminal	−12.4	−15.2	2.144	2.310	2.098	---	2.028	2.133	2.083	1.631	–	1.034	–	1.878	–
P1B_4_bridge	−27.6	−25.7	2.140	1.160	2.107	---	2.077	2.205	2.118	1.590	–	1.027	–	2.037	2.103

Such a large energy difference (ca. 24 kcal/mol) between the ***anti*_P1A_3** and ***anti*_P1B_3_terminal** products could be explained by presence of a five-coordinated Zr^1 center in the ***anti*_P1B_3_terminal** (see Figure 4). Since the coordination of five ligands to the Zr center is not thermodynamically suitable, Zr^1 releases either the amido (RN^3) or H^2 ligand to form a four-coordinated environment, called RN- and H-migration steps, respectively. The released amido (RN^3) or H^2 ligand moves to bridging position between two Zr centers and leads to ***anti*_P1A_3** and ***anti*_P1B_3_bridge** structures. Calculations show that the ***anti*_P1B_3_terminal** → ***anti*_P1A_3** isomerization occurs with only 0.2−0.3 kcal/mol energy barrier (the transition state corresponding to this process is presented in Supporting Information) and is exothermic by 24.1 kcal/mol. Meanwhile, the ***anti*_P1B_3_terminal** → ***anti*_P1B_3_bridge** isomerization occurs with a slightly larger barrier (1−2 kcal/mol) and is only 11.5 kcal/mol exothermic. Thus, the direct product of N-side addition of the H_2 molecule, the intermediate ***anti*_P1B_3_terminal**, can easily (kinetically and thermodynamically) rearrange to the Cp-side addition product ***anti*_P1A_3** with RN(amido)-bridge. However, the formation of the energetically less favorable structure ***anti*_P1B_3_bridge** during the reaction *anti*-**3**-(μ_2,η^2,η^2-N_2)-**3** + H_2 cannot be excluded.

Reactivity of *syn*-n-(μ_2,η^2,η^2-N_2)-n toward the Dihydrogen Molecule. Now, let us discuss the mechanism of the reaction of *syn*-**n**-(μ_2,η^2,η^2-N_2)-**n** with the H_2 molecule. As seen from Figure 2, for the *syn*-**n**-(μ_2,η^2,η^2-N_2)-**n** complex, the Cp-side

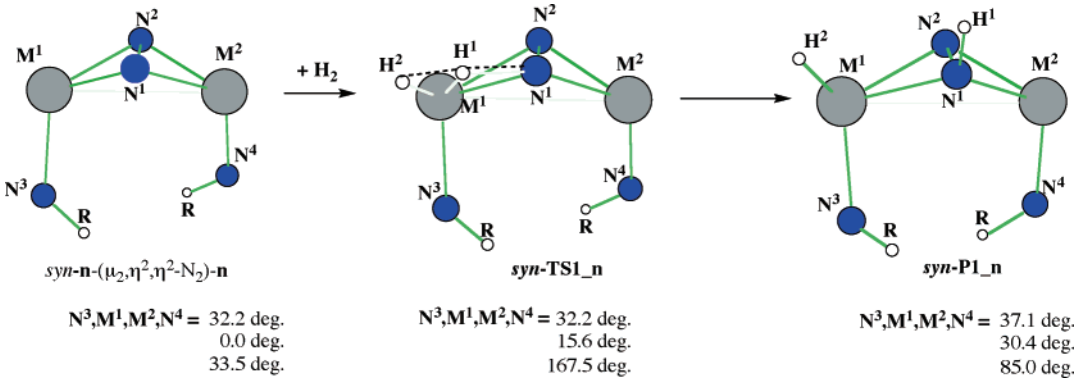

Figure 5. Schematic presentation of the reactants, intermediates, transition states, and products of the reaction of *syn*-**n**-(μ_2,η^2,η^2-N_2)-**n** with H_2 molecule. The calculated, important geometry parameters and relative energies of these complexes are presented in Table 5.

Table 5. Calculated, Important Geometry Parameters (distances in Å, and angles in deg, see also Figure 5), and Relative Energies (in kcal/mol), ΔH (in gas-phase) and ΔG_{Sol} (in water solution), of the Reactants, Transition States, Intermediates, and Products of the Reaction of *syn*-n-(μ_2,η^2,η^2-N_2)-n with H_2 Molecule (where n = 1, 3, and 4)

structure	ΔH	ΔG_{Sol}	M^1-N^1	M^1-N^2	M^1-N^3	M^2-N^3	M^2-N^1	M^2-N^2	M^2-N^4	N^1-N^2	H^1-H^2	N^1-H^1	M^1-H^1	M^1-H^2
1-(μ_2,η^2,η^2-N_2)-**1**	0.0	0.0	1.871	1.941	1.949	–	1.941	1.871	1.949	1.494	–	–	–	–
TS1A_1	19.8	19.2	2.094	1.947	1.941	–	1.938	1.876	1.949	1.487	1.016	1.331	1.874	1.867
P1A_1	−7.6	−16.3	2.112	1.981	1.957	–	1.974	1.854	1.934	1.490	–	1.029	–	1.712
3-(μ_2,η^2,η^2-N_2)-**3**	0.0	0.0	2.037	2.063	2.105	–	2.063	2.037	2.105	1.576	–	–	–	–
TS1A_3	14.1	18.5	2.171	2.077	2.104	–	2.029	2.057	2.103	1.597	0.975	1.411	2.081	2.109
P1A_3	−18.6	−9.3	2.257	2.128	2.111	–	2.126	2.012	2.085	1.534	–	1.029	–	1.895
4-(μ_2,η^2,η^2-N_2)-**4**	0.0	0.0	2.032	2.075	2.101	–	2.075	2.032	2.101	1.558	–	–	–	–
TS1A_4	17.7	20.1	2.217	2.095	2.083	–	2.063	2.048	2.105	1.547	1.056	1.357	1.988	2.024
P1A_4	−30.7	−26.1	2.162	2.053	2.350	2.307	2.186	2.091	2.351	1.511	–	1.025	–	1.905

attack of H_2 looks electronically and sterically to be the more favorable pathway.

As seen in Table 5 and Figure 5, the *syn*-isomer of **n**-(μ_2,η^2,η^2-N_2)-**n**, (where **n** = **1**, **3**, and **4**) reacts with the first H_2 molecule with an energy barrier similar to those for their corresponding *anti*-isomers. For **n** =**1** the calculated barrier is 19.8 kcal/mol, while it reduces to 14.1 and 17.7 for complexes **n** = **3** and **4**. Close inspection of the transition states, ***syn*-TS1_n**, associated with these barriers (see Figure 5 and Table 5) reveals that for **n** = **4** (M = Zr and R = Me) it has a structure similar to that of its *anti* counterpart. Indeed, the calculated (N^3,M^1,M^2,N^4) dihedral angle is 167.5°. In other words, addition of an H_2 molecule causes rotation of one of the ($CpSiH_2NMe$)Zr groups around the Zr−Zr bond. This can be explained in terms of strong steric repulsion between the RN−NR groups. Indeed, in the complex **n** = **3** (M = Zr and R = H), where steric repulsion between the HN−NH groups is smaller, this effect is not significant ((N^3,M^1,M^2,N^4) dihedral angle is only 15.6°).

The reaction *syn*-**n**-(μ_2,η^2,η^2-N_2)-**n** + H_2 → ***syn*_P1_n** is calculated to be exothermic by 7.6, 18.6, and 30.7 kcal/mol for **n** = **1**, **3**, and **n** = **4**, respectively. Analysis of the optimized structures of ***syn*_P1_n** products shows that ***syn*_P1_4** has a structure similar to that for ***anti*_P1A_4**, while structures of ***syn*_P1_1** and ***syn*_P1_3** are very different from their *anti* counterparts. These findings are consistent with the calculated exothermicity of the reactions, *anti*-**4**-(μ_2,η^2,η^2-N_2)-**4** + H_2 → ***anti*_P1A_4** and *syn*-**n**-(μ_2,η^2,η^2-N_2)-**n** + H_2 → ***syn*_P1_n** for **n** = **4**; they have very similar exothermicities, but for **n** = **1** and **3** the formation of the *syn*-product is significantly less exothermic.

The studies of the mechanism of the ***syn*_P1_n** → ***anti*_P1A_n** isomerization reaction, as well as of the H_2 (the second) addition to ***syn*_P1_n** and ***anti*_P1A_n** products are in progress and will be discussed elsewhere.

4. Solvent Effects

As seen in Tables 4 and 5, inclusion of the bulk solvent effect (water was chosen as a solvent) into the calculations did not change the above-presented trends from the gas-phase studies. Indeed, solvent effects only slightly change the calculated barriers for the reaction of ***anti*-1**-(μ_2,η^2,η^2-N_2)-**1** and ***syn*-1**-(μ_2,η^2,η^2-N_2)-**1** with the H_2 molecule, while it makes these reactions more exothermic by a few kcal/mol. For Zr-complexes **3** and **4**, inclusion of solvent effects increases the calculated barriers by 2−3 kcal/mol and reduces the exothermicity of the studied reactions. However, still the calculated H_2 addition barrier remains a few kcal/mol smaller for Zr-complexes compared to that for their Ti-analogues.

5. Conclusions and Summary

The above-presented results clearly show that (1) all studied species **n** = **1**, **2**, **3**, **4**, **5**, and **6** preferentially coordinate N_2 molecule in the side-on manner and form the highly stable (relative to the dissociation limit of 2**n** + N_2) **n**-(μ_2,η^2,η^2-N_2)-**n** complex. Thus, the resultant **n**-(μ_2,η^2,η^2-N_2)-**n** complex satisfies the first necessary condition of hydrogenation of the coordinated N_2 molecule; (2) both *anti*- and *syn*-isomers of the **n**-(μ_2,η^2,η^2-N_2)-**n** complex satisfy the second necessary condition for the successful hydrogenation of the coordinated N_2 molecule; both isomers possess appropriate frontier orbitals: HOMO is a π-bonding orbital of the M−N_2−M fragment, while the LUMO has mainly a metal character. Therefore, it could be expected that (3) all studied **n**-(μ_2,η^2,η^2-N_2)-**n** complexes add the H_2 molecule with a reasonable barrier (ca. 20, 14−16, and 15−18 kcal/mol barriers for **n** = **1**, **3**, and **4**, respectively) regardless of the direction of H_2 attack (Cp- or N-side) and the nature of initial complex (*anti* or *syn*). However, the Zr-complex (**n** = **3**) is expected to be more reactive than its Ti-analogue (**n** = **1**), and replacement of R = H ligand with R= Me (i.e., going from **n** = **3** to **n** = **4**) has no significant effect on the calculated

barriers. The comparison of the calculated H−H addition barriers of these reactions with those (18−20 and 24 kcal/mol barriers) for the experimentally,[15,16] and computationally[2−5,10−14] well-studied dizirconium complexes $\{[P_2N_2]Zr\}_2(\mu_2,\eta^2,\eta^2\text{-}N_2)$ and $\{(C_5Me_4H)_2Zr\}_2(\mu_2,\eta^2,\eta^2\text{-}N_2)$ show that the proposed complexes **1**, **3**, and **4** should exhibit similar or better reactivity toward the first H_2 molecule than the latter complexes do. (4) It was shown that, in general, reaction *anti*-**n**-$(\mu_2,\eta^2,\eta^2\text{-}N_2)$-**n** + $\mathbf{H_2}$ → ***anti*_P1A_n** leading to the product with H- or NR-bridge is more exothermic than its *syn*-counterpart, *syn*-**n**-$(\mu_2,\eta^2,\eta^2\text{-}N_2)$-**n** + $\mathbf{H_2}$ → ***syn*_P1_n** leading to nonbridged products. The first reaction is calculated to be exothermic by ca. 23.0, 35.5, and 32.4 kcal/mol, while the second reaction is exothermic only by 7.6, 18.6, and 30.7 kcal/mol, for **n** = **1**, **3**, and **4**, respectively. (5) The inclusion of solvent (water) effects into the calculations did not change trends and conclusions obtained from the gas-phase studies.

In summary, the results presented above clearly show that the proposed $(CpSiH_2NR)M\text{-}(\mu_2,\eta^2,\eta^2\text{-}N_2)\text{-}M(CpSiH_2NR)$, complex (for M = Zr and Ti, and R = H, Me, ^{t}Bu) are likely to exhibit similar or better reactivity toward the H_2 molecule than the experimentally,[15,16] and computationally[2−5,10−14] well-studied dizirconium complexes $\{[P_2N_2]Zr\}_2(\mu_2,\eta^2,\eta^2\text{-}N_2)$ and $\{(C_5Me_4H)_2Zr\}_2(\mu_2,\eta^2,\eta^2\text{-}N_2)$. We encourage experimentalists to examine these predictions. One should note that studies of the mechanism of ***syn*_P1_n** → ***anti*_P1A_n** isomerization, as well as of the H_2 (the second) addition to ***syn*_P1_n** and ***anti*_P1A_n** products are in progress and will be discussed elsewhere.

Acknowledgment. S.M. thanks Spanish MEC and CICYT (MAT2006-0400 Project) for financial support. We thank AFOSR for DURIP Grant (FA9550-04-1-0321) for support of the computer facilities. The use of computational resources at the Cherry Emerson Center for Scientific Computation is also acknowledged.

Supporting Information Available: Complete ref 22; Table S1, Cartesian coordinates (Å) of all reported structures; Tables S2−S7, calculated energetics (au) of all reported structures; and Figure S1, HOMO and LUMO of ***syn*-n-$(\mu_2,\eta^2,\eta^2\text{-}N_2)$-n** complexes (**n** = **1**, **3**, and **4**). This material is available free of charge via the Internet at http://pubs.acs.org.

OM700613V